Hindawi
Advances in Materials Science and Engineering
Volume 2020, Article ID 8845366, 12 pages
https://doi.org/10.1155/2020/8845366

Research Article

Sorptive Removal of Color Dye Safranin O by Fibrous Clay Minerals and Zeolites

Ben Sieren,[1] Jessica Baker,[1] Xisen Wang,[2] Samuel J. Rozzoni,[2] Kristen Carlson,[1] Alyssa McBain,[1] Daniel Kerstan,[1] Lori Allen,[2] Libing Liao,[3] and Zhaohui Li[1]

[1]*Department of Geosciences, University of Wisconsin–Parkside, 900 Wood Road, Kenosha, WI 53144, USA*
[2]*Department of Chemistry, University of Wisconsin–Parkside, 900 Wood Road, Kenosha, WI 53144, USA*
[3]*Beijing Key Laboratory of Materials Utilization of Nonmetallic Minerals and Solid Wastes, National Laboratory of Mineral Materials, School of Materials Science and Technology, China University of Geosciences, Beijing, 29 Xueyuan Road, Beijing 100083, China*

Correspondence should be addressed to Libing Liao; lbliao@cugb.edu.cn and Zhaohui Li; li@uwp.edu

Received 6 September 2020; Revised 11 November 2020; Accepted 13 November 2020; Published 2 December 2020

Academic Editor: Matjaz Valant

The increased use of color dyes in industry imposes a great threat to the environment. As such, developing cost-effective techniques for dye removal from wastewater attracted great attention. Earth materials, particularly those with large specific surface area (SSA) and high cation exchange capacity (CEC), were evaluated for their potential use for wastewater treatment. In this study, palygorskite, sepiolite, and clinoptilolite were evaluated for their removal of cationic dyes using safranin O (SO^+) as a model compound. The CEC values of the materials played a key role in SO^+ removal while other physicochemical conditions, such as temperature, equilibrium solution pH, and ionic strength, had less influence on SO^+ removal. Sorbed SO^+ cations were limited to the external surfaces of the minerals, as their channel sizes are less than the size of SO^+ cation. Molecular dynamic simulations showed dense monolayer SO^+ uptake on palygorskite due to its relatively large CEC value. In contrast, loosely packed monomer SO^+ uptake was adopted on sepiolite for its large SSA and low CEC. Dense multilayers or admicelles of SO^+ formed on zeolite surfaces. As such, for the best SO removal, palygorskite is better than sepiolite, though both are fibrous clay minerals.

1. Introduction

Pigments and dyes are widely used in different types of industries including textile and leather dyeing, paper, printing, pharmaceutical, and cosmetics [1]. As such, large-scale production and widespread applications resulted in many synthetic organic dyes to permeate into different compartments of water and soil bodies [2]. To prevent direct discharges of waters containing different types, amounts, and toxicities of dyes that threaten the environment, numerous studies were conducted recently to treat the dye-containing water [3]. However, as there are more than 10,000 types of dyes used and each may have different physicochemical properties [4], and different approaches were undertaken for dye removal including physical [3], chemical [4], and biological [5], effective methods for removal of a particular dye might be limited. In addition, most of the studies were focused on developing new materials, mostly nanomaterials [3, 6], due to their large specific surface area (SSA) and high reactivity. However, high material costs may limit their immediate practical values.

Earth materials have long been used to sorb color dyes for painting purposes. A typical example is Maya blue, a mixture of indigo dyes with palygorskite, used to color sculpture, artwork, and textiles around the Aztec area in Mexico over 1200 years. Due to the skyrocketing use of color dyes and inexpensive material cost, earth material was studied extensively for the removal of color dyes, most of them were of cationic and zwitterionic in nature, from solution because of large SSA and high cation exchange capacity (CEC) of many phyllo- and tectosilicates, such as different types of clay minerals and zeolites.

Safranin O (SO), also called Basic Red 2, Cotton Red, Gossypimine, Safranin T, and Safranin Y or A, is a water-soluble reddish-brown powder [7], commonly used in tracer and biological laboratory purposes [8]. As such, methods tested for its removal from water include physicochemical, biological, and chemical methods [9].

Studies on SO removal by clay minerals were limited. Montmorillonite (MMT), due to its high CEC and SSA values, could sorb SO to a capacity of 380 mg/g or 1.1 mmol/g [10]. In a different study, SO removal capacity by bentonite collected from Khulais, Saudi Arabia, was 294 mg/g or 1.1 mmol/g [11], but neither the CEC value of the clay nor the mechanism of SO removal was discussed. An SO removal capacity of 24 mg/g or 68 mmol/kg was reported for a Saudi Arabia natural clay [8]; however, the major components of the clay were quartz, chamosite, albite, dickite, and microcline as determined by X-ray diffraction analyses, and the mechanism of SO removal was not mentioned.

SO sorption capacity on kaolinite was up to 16 mg/g or 45 mmol/kg as reported in one study [12]. On a different kaolinite, SO sorption capacity as high as 160 mmol/kg was also reported, and the relatively hydrophobic silica face of kaolinite contributed more to the SO sorption and aggregation [13]. SO sorption on a raw ferruginous kaolinite was up to 59.3 mg/g or 168 mmol/kg and was attributed to physical behavior, heterogeneous nature, and multilayer formation [14].

Palygorskite (PAL) and sepiolite (SEP) are fibrous phyllosilicates. Both have channels running parallel to the fiber length with channel sizes of 0.37 by 0.64 nm for SEP and 0.37 by 1.06 nm for SEP that are accessible by inorganic cations [15]. Thus, not only the surfaces but also the channel area is responsible for cation exchanges and specific sorption of cations. In one study, an SO sorption capacity of 200 mg/g was found on a natural Iraqi PAL, but the CEC value of the PAL was not reported [16]. No studies of SO sorption on natural sepiolite were reported, but an SO sorption capacity of 18.48 mg/g was reported on iron oxide/sepiolite magnetite composite (MSep) [17].

Zeolite is a group of minerals in tectosilicates with abundant resources, available globally, and has already found many applications because of its high CEC and SSA [18]. A clinoptilolite zeolite (CZ) was studied for the sorption and release of photodynamically active dyes hypericin (Hyp), methylene blue (MB), chlorin e6, Alphthalocyanine, and fluorescein under multiphoton microscopy, and the results suggested even distribution of the dyes on the surface of CZ with the potential release of Hyp from CZ surfaces in the presence of biomolecules, indicating that CZ could serve as an effective material for drug delivery and controlled release in biological systems [19]. Sorption of SO on CZ showed a capacity of 0.08 mg/g, and the sorption increased with initial solution pH [20], but the mechanism was not discussed. In a different study, even for the CZ modified by iron oxide nanoparticles, the MB sorption capacity was still at 52 mg/g, corresponding to 170 mmol/kg, and again, the mechanism of MB removal was not discussed [21]. Sorption of SO on a CZ from Yemen resulted in a capacity of 43 mg/g or 120 mmol/kg, and the SO uptake on ZEO was attributed to cation exchange and chemisorption [22]. On the opposite, after acid modification, the uptake of a color dye Red 24 on a CZ was only 0.9 mmol/kg [23]. A magnetic zeolite NaA achieved an SO removal capacity of 149 mg/g or 425 mmol/kg after sodium dodecyl sulfate (SDS) modification [18], while the purpose of SDS coating was not mentioned, nor noncoating zeolite as controls was compared.

This study aims to use the selected phyllo- and tectosilicates with open channels to assess their SO removal from water under different physicochemical conditions and to correlate changes in material properties of the sorbents after SO uptake as characterized by different instruments. In addition, the interactions between SO and the minerals were simulated by molecular dynamic simulations. The configuration of sorbed SO^+ cations on the mineral surfaces was derived from the sorption study and instrumental analyses in conjunction with the simulation. Then, the SO removal mechanism by the minerals was proposed.

2. Materials and Methods

2.1. Materials. The SO used is in a chloride form (CAS number of 477-73-6, $M = 350.84$ g/mol). Literature values are 50 g/L for solubility [24] and 11 for pKa [13]. Molecular sizewise, it is 1.16 nm long by 0.96 nm wide by 0.4 nm thick, as determined by a molecular editor Avogadro (https://avogadro.cc/) (Figure 1).

The minerals used include fibrous phyllosilicates palygorskite (PAL) and sepiolite (SEP) and tectosilicate zeolite (ZEO), all with channel structures where sorption of inorganic cations is attainable. The PAL used is PFl-1, and the SEP used is SepSp-1. Both were reference clays obtained from the Source Clay Minerals Repository. The ZEO used is clinoptilolite obtained from the St. Cloud Mine in Winston, NM. The CEC values are 175 [25] and 15 [26] meq/kg, for PFl-1 and SpeSp-1, respectively, while their SSA values are 173 [27] and 250 m^2/g [26]. For ZEO, the external CEC (ECEC) is 90 meq/kg and the SSA is 15.7 m^2/g [28].

2.2. SO Uptake. For SO removal by PAL and ZEO, 0.25 g of solid and 10 mL of SO solution were added to each 50 mL centrifuge tube. For SEP, 0.5 g of solid and 10 mL of solution were used due to its lower CEC value. The initial concentrations for the isotherm study varied from 0.3 to 2.5 mM for ZEO and SPE and up to 5 mM for PAL, and the mixtures were shaken on a reciprocal shaker at 150 rpm and room temperature ($23 \pm 1^\circ$C) for 24 h. For the kinetic study, mixing lasted from 0.1 to 24 h. To investigate the influence of solution pH on SO removal, the equilibrium pH was adjusted multiple times during the 24 h period to achieve final values between 3 and 11 with an interval close to 1. For the influence of solution ionic strength on SO removal, the SO solution was made with 0.001, 0.01, 0.1, and 1.0 M of NaCl instead of DI water. The influence of temperature on SO removal was tested at 23, 33, 43, and 53°C with a deviation of less than 1°C. In all these studies, the initial SO concentrations were fixed at 4.5, 2.0, and 1.0 mM for PAL, ZEO, and

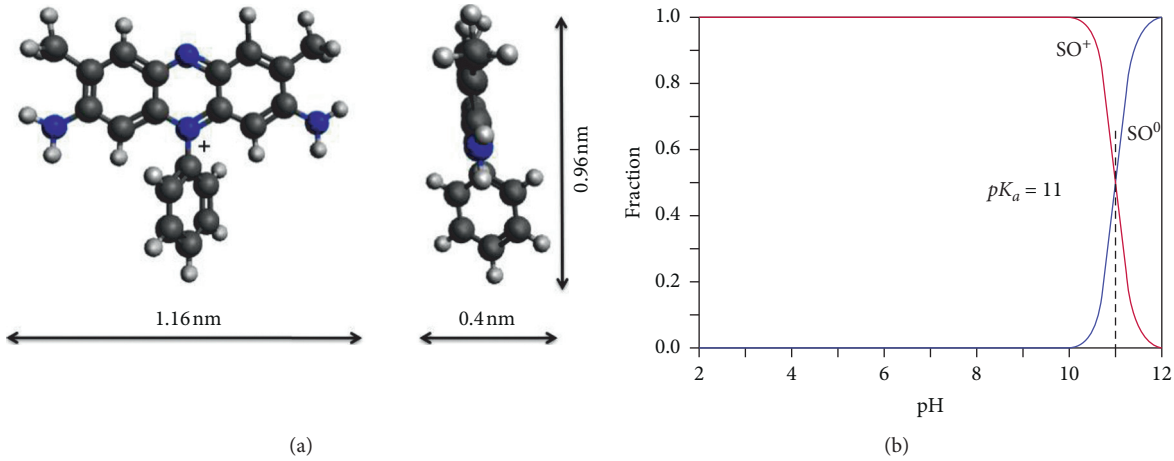

FIGURE 1: Molecular structure of SO viewed from different directions (a) and its pH speciation (b).

SEP, respectively, and shaken for 24 h. After mixing, samples were centrifuged at 3500 rpm for 10 min and the supernatants passed through 0.45 μm syringe filters before being analyzed for equilibrium SO concentrations using a UV-Vis method. The amount of SO sorbed was determined by the difference between the initial and equilibrium SO concentrations. Duplicates were tested for each experimental condition.

2.3. Instrumental Analyses. The equilibrium SO concentrations were determined by a UV-Vis spectrophotometer. The wavelength used was 516 nm [29, 30]. To assess the counterion Cl^-concentration in solution, an ion chromatography (IC) with a PRP-100 anion exchange column was used. Calibration was made using SO concentrations of 0.1 to 5 mM with an r^2 of 0.999.

A Shimadzu 6100 X-ray diffractometer was used for X-ray diffraction (XRD) analyses of the samples after sorption experiments. A Ni-filtered CuKα radiation at 30 kV and 40 mA and a scanning speed of 2°min were set for the experimental conditions, and the samples were scanned from 5 to 40° (2θ). The FTIR spectra were acquired on a Shimadzu IRAffinity-1S FTIR spectrometer equipped with a quartz attenuated total reflection device from 400 to 4000 cm^{-1} with a resolution of 4 cm^{-1}.

2.4. Molecular Dynamic Simulation. The molecular dynamic simulation was performed using the FORCITE module in Materials Studio 6.0 software to determine the surface configurations of sorbed SO^+ cations on different surfaces of the minerals. The number of SO^+ cations used for the simulation was based on the SSA of the minerals and the SO sorption capacity on each mineral. The unit cell parameters used were as follows: $a = 12.78$ Å, $b = 17.86$ Å, $c = 5.24$ Å, $\beta = 95.78°$, and $Z = 4$ for PAL; $a = 13.43$ Å, $b = 26.88$ Å, $c = 5.281$ Å, and $Z = 4$ for SEP; and $a = 17.688$ Å, $b = 17.902$ Å, $c = 7.409$ Å, $\beta = 116.5°$, and $Z = 4$ for ZEO. Also, the supercells were made of 2*bx*4*c* for PAL and SEP due to their layered structure and 2*bx*4*c*, 2*ax*4*c*, and 2*ax*1.5*b* for ZEO due to its 3D structure. The constructed model was optimized geometrically.

3. Results and Discussion

3.1. Kinetics of SO Removal. SO removal by these minerals was relatively fast, and equilibrium could be reached within an hour for PAL and SEP (Figure 2(a)). In contrast, it may take up to 8 h to reach equilibrium for ZEO. This could be due to its larger particle size, and thus, longer diffusion time is needed to reach equilibrium. Similarly, uptake of SO on CMC-41 was thought as diffusion controlled [7]. The results were fitted to several kinetic models, and the pseudo-second-order kinetics fitted the data best. It has the following form:

$$q_t = \frac{kq_e^2 t}{1 + kq_e t}, \quad (1)$$

that can be rearranged into a linear form as follows:

$$\frac{t}{q_t} = \frac{1}{kq_e^2} + \frac{1}{q_e} t, \quad (2)$$

where k (kg/mmol-h) and kq_e^2 (mmol/kg-h) are the rate constant and initial rate of SO removal by the minerals, while q_t and q_e (mmol/kg) are the amount of SO uptake at time t and at equilibrium. The initial rates and the rate constants are 1379, 213, and 23256 mmol/kg-h and 3.5, 0.04, and 0.7 kg/mmol-h for SO uptake on SEP, ZEO, and PAL, respectively. Meanwhile, calculated q_e values were 20, 76, and 180 mmol/kg for SO uptake on SEP, ZEO, and PAL, respectively, with the coefficients of determination r^2 all greater than 0.999 (inset of Figure 2(a)). The very high rate, large rate constant, and larger q_e for SO uptake on PAL correlated to its larger CEC and SSA values well. In comparison, the slow SO removal by ZEO confirmed the speculation that diffusion played an important role. In a previous study, SO sorption on MSep followed the pseudo-second-order kinetics with a k of 0.19 g/mg-min [17].

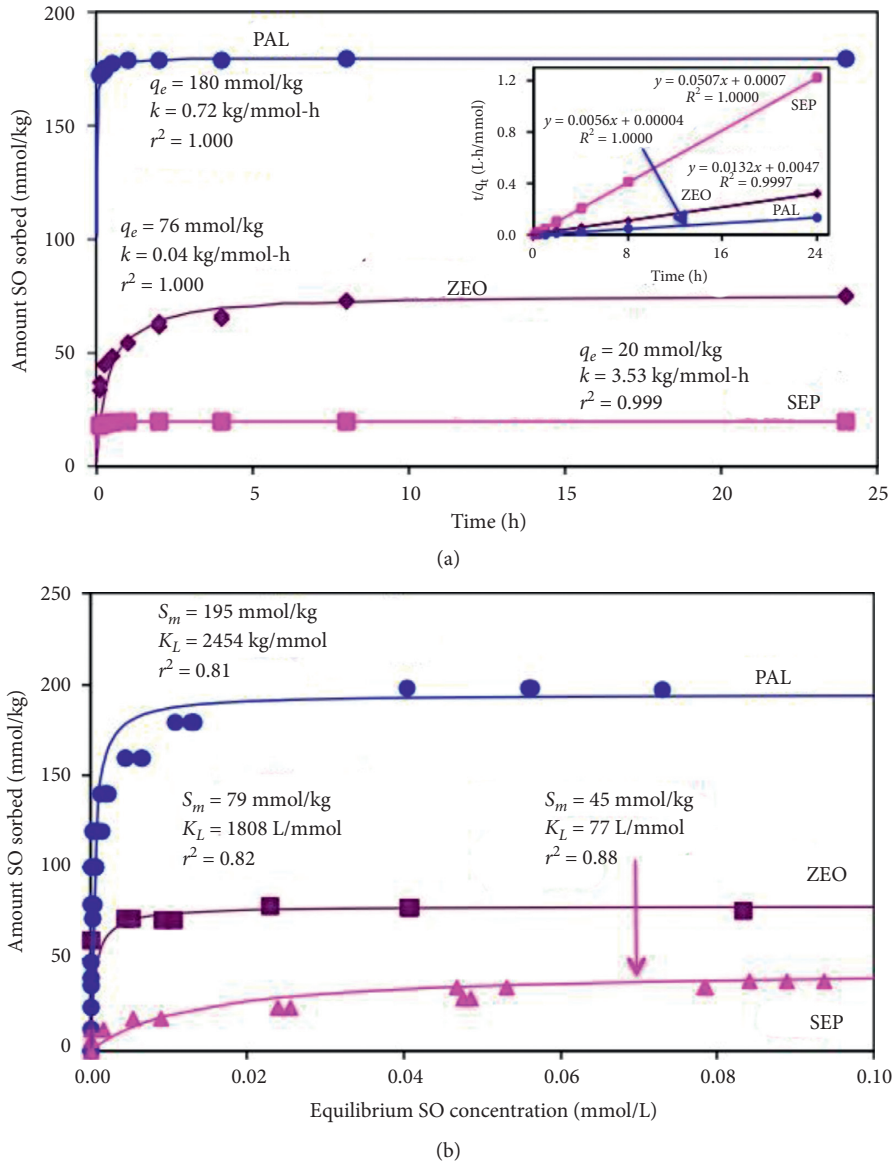

Figure 2: Kinetics (a) and isotherm (b) of SO sorption on PAL, ZEO, and SEP. The lines are pseudo-second-order (a) and Langmuir (b) fits the experimental data. Inset in (a) is linearized fit to the pseudo-second-order kinetics.

3.2. Isotherms of SO Uptake. Uptake of SO by the tested minerals is illustrated in Figure 2(b). Results were fitted to both the Freundlich and Langmuir models, and the latter had a better fit. The Langmuir isotherm has the following form:

$$C_s = \frac{K_L S_m C_L}{1 + K_L C_L}, \tag{3}$$

that can be converted into a linear form as follows:

$$\frac{C_L}{C_s} = \frac{1}{K_L S_m} + \frac{C_L}{S_m}, \tag{4}$$

where C_L and C_S are the equilibrium SO concentration in solution (mmol/L) and amount of SO sorbed on solid (mmol/kg), while S_m (mmol/kg) and K_L (L/mmol) are the Langmuir parameters corresponding to the SO sorption capacity and SO affinity for the minerals. The fitted results are S_m = 195, 79, and 45 mmol/kg and K_L = 2450, 1808, and 77 L/mmol for SO sorption on PAL, ZEO, and SPE, respectively. The CEC values of PFL and SEP are 175 [25] and 15 [26] meq/kg. For ZEO, the ECEC value is 90 meq/kg [28].

A previous study showed an SO sorption capacity of 200 mg/g or 570 mmol/kg on PAL [16]. Sorption of MB on a PAL showed a capacity of 200 mmol/kg [31]. However, the CEC and SSA values and the purity of the mineral in these studies were not provided. Moreover, the data in their isotherm study only showed a capacity slightly over 100 mg/g or about 300 mmol/kg [16]. SO sorption on MSep also followed the Langmuir isotherm with a sorption capacity of 18.48 mg/g [17]. In a previous study, the SO uptake on CZ was 43 mg/g or 120 mmol/kg and was attributed to cation exchange and chemisorption [22]. The SO sorption on a synthetic ZEO was only 9.4 mg/g [32]. On a different type of

ZEO, the SO sorption only reached a capacity of 1.3 mg/g [33]. Even lower, sorption of SO on CZ was fitted to the Langmuir isotherm with a capacity of 0.055 mg/g, corresponding to only 0.155 mmol/kg [20], in comparison with 79 mmol/kg in this study (Figure 2(b)).

As the SO used is SO^+Cl^-, the equilibrium counterion Cl^-concentrations at the SO sorption capacity were about 30% lower than their initial concentrations as measured by ion chromatography, suggesting that some of the SO removal from solution was in a dimeric form balanced by counterion Cl^-bridging the two cations. An increase in dimer concentration was associated with increased SO concentration [34].

For CZ, there are three channels of which two channels are running parallel to each other and to the *c*-axis with a channel consisting of a 10-member ring of a size of 0.44–0.72 nm and another channel consisting of an 8-member ring of a size of 0.41–0.47 nm, while the third channel is parallel to *a*-axis and made of an 8-member ring of a size of 0.40–0.55 nm [35]. As the size of SO is greater than the channel size of the three channels, the uptake of SO is limited to the external surfaces of ZEO. Taking consideration of the limited SSA, the uptake of SO may form a multilayer sorption on ZEO.

3.3. Influence of Solution pH, Ionic Strength, and Temperature on SO Uptake. Essentially, equilibrium solution pH had minimal influence of SO uptake on these minerals (Figure 3(a)). A similar pH effect on SO removal by PAL was reported earlier [16]. As the initial solution pH increased from 2 to 10, the amount of SO sorption on CZ increased from 3.5 to 7 mg/g [20]. Similarly, the SO uptake on ZEO increased from 30 to 60% as the initial solution pH increased from 2 to 10 [33]. A slight increase in SO removal from 82 to 95% was observed for a Yemen CZ [22]. With a pK_a value of 11, SO is in a cationic form when equilibrium solution pH is <11. The negligible pH influences on SO^+ uptake indicated that organic cations have a higher affinity for negatively charged mineral surfaces in comparison with inorganic cations.

Similar to equilibrium solution pH, solution ionic strength also had a minimal influence of SO uptake (Figure 3(b)). A previous study showed that added NaCl, $CaCl_2$, Na_2SO_4, and NH_4Cl in the range of 0–10% (w/v) also had minimal influence on SO uptake on modified zeolite [18]. The results suggested again that the organic cation had higher affinity for the negatively charged mineral surfaces in comparison with inorganic cations.

Influence of equilibrium temperature on SO uptake revealed exothermic processes for SO removal using PAL, ZEO, and SEP (Figure 3(c)). The thermodynamic parameters of SO removal can be related to the SO distribution coefficient K_d, the ratio of SO sorbed on solids to the equilibrium SO concentration in solution, by

$$\ln K_d = -\frac{\Delta H}{RT} + \frac{\Delta S}{R}, \quad (5)$$

where the ΔH and ΔS are the changes in enthalpy and entropy after SO uptake, R is the gas constant, and T is the temperature in K. The ΔH and ΔS values are related to the free energy ΔG of SO uptake by

$$\Delta G = \Delta H - T\Delta S. \quad (6)$$

The thermodynamic parameters of SO calculated from equations (5) and (6) showed small ΔS° values, moderate negative ΔH°, and ΔG° values in the ranges of −14 to −24 kJ/mol (Table 1), indicating net attractive interactions via physical sorption or electrostatic interactions between the solute and sorbents. The ΔG° value was about −15 kJ/mol for SO uptake on MSep, suggesting physisorption [17].

3.4. XRD Analyses. The SO used is crystalline as revealed by the XRD analysis (Figure 4 inset). None of the SO peaks showed up in the XRD patterns of the three minerals after uptake of different amounts of SO, confirming that the SO uptake from solution was via sorption instead of precipitation. Meanwhile, the *d*-spacings of the minerals did not change after SO uptake, indicating the location of sorbed SO^+ cations was limited to the external surfaces, although all three minerals have channel structures where the sites for the uptake of inorganic cations are available (Figure 4).

3.5. FTIR Analyses. The full FTIR spectra of the three minerals together with the crystalline SO are displayed in Figure 5. For SO, the broad absorption bands at 3338 and 3183 cm^{-1} were assigned to the –OH and–NH_2 groups and to the N–H group [36]. However, in this study, they are located at 3313 and 3140 cm^{-1} (Figure 5). In a different study, bands at 1641 and 1610 cm^{-1} were assigned to the aromatic ring stretching vibration, 1493 cm^{-1} to the –CH_3 stretching vibration, and 1334 cm^{-1} to the aromatic C = N stretching vibration [37]. These bands were located at 1639, 1609, 1485, and 1323 cm^{-1} in this study (Figure 5). Meanwhile, the C = N stretching vibration band was located at 1320 cm^{-1} [38].

These bands did not show up after SO uptake on PAL from the initial SO concentration of 0.9 mM, corresponding to an SO uptake of 36 mmol/kg, except the one at 1323 cm^{-1}. At an initial concentration of 2.0 mM, corresponding to an SO uptake of 80 mmol/kg, the bands at 1485 and 1528 cm^{-1} started to appear and shifted to 1489 and 1533 cm^{-1}. Meanwhile, the band at 1323 cm^{-1} shifted to 1337 cm^{-1} (Figure 6(a)). At the SO sorption capacity of 198 mmol/kg, the bands remained at the same location (no further band shift was observed), but their intensities increased accordingly. For SEP, the only band showed up was the one at 1323 cm^{-1}, even at the highest SO input concentration of 2.5 mM, corresponding to an SO uptake of 43 mmol/kg, and the band shifted to 1331 cm^{-1} after SO uptake on SEP (Figure 6(b)). For ZEO, the 1323 cm^{-1} band showed up at an initial concentration of 0.9 mM, corresponding to an SO uptake of 36 mmol/kg, and the bands at 1323, 1485, 1533, and 1609 cm^{-1} all appeared at the SO initial concentration of 1.5 mM, corresponding to an SO uptake of 60 mmol/kg, and

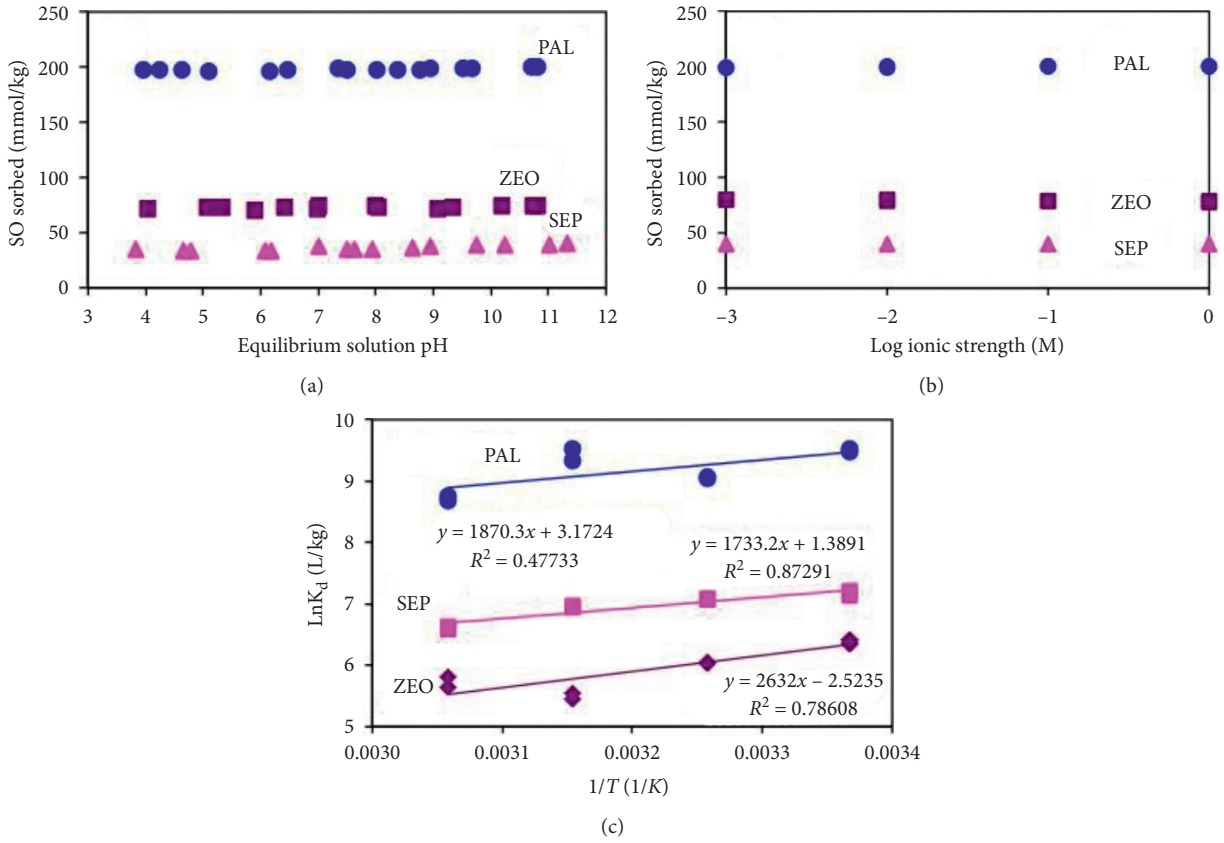

Figure 3: Influence of equilibrium solution pH (a), ionic strength (b), and temperature (c) on SO sorption on PAL, ZEO, and SEP.

Table 1: Thermodynamics of SO uptake on PAL, ZEO, and SEP.

Minerals	ΔG° (kJ/mol)				ΔH° (kJ/mol)	ΔS° (kJ/mol-K)
	296 K	306 K	316 K	326 K		
ZEO	−15.7	−15.5	−15.3	−15.0	−21.9	−0.02
SEP	−17.8	−17.9	−18.1	−18.2	−14.4	0.01
PAL	−23.4	−23.6	−23.9	−24.1	−15.6	0.03

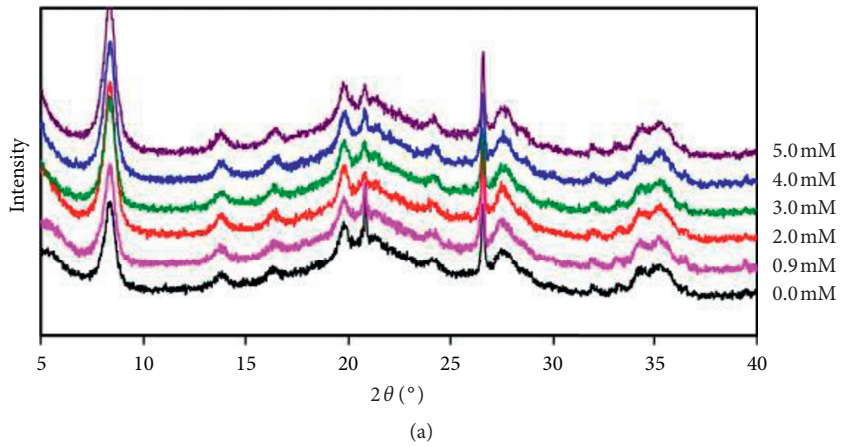

Figure 4: Continued.

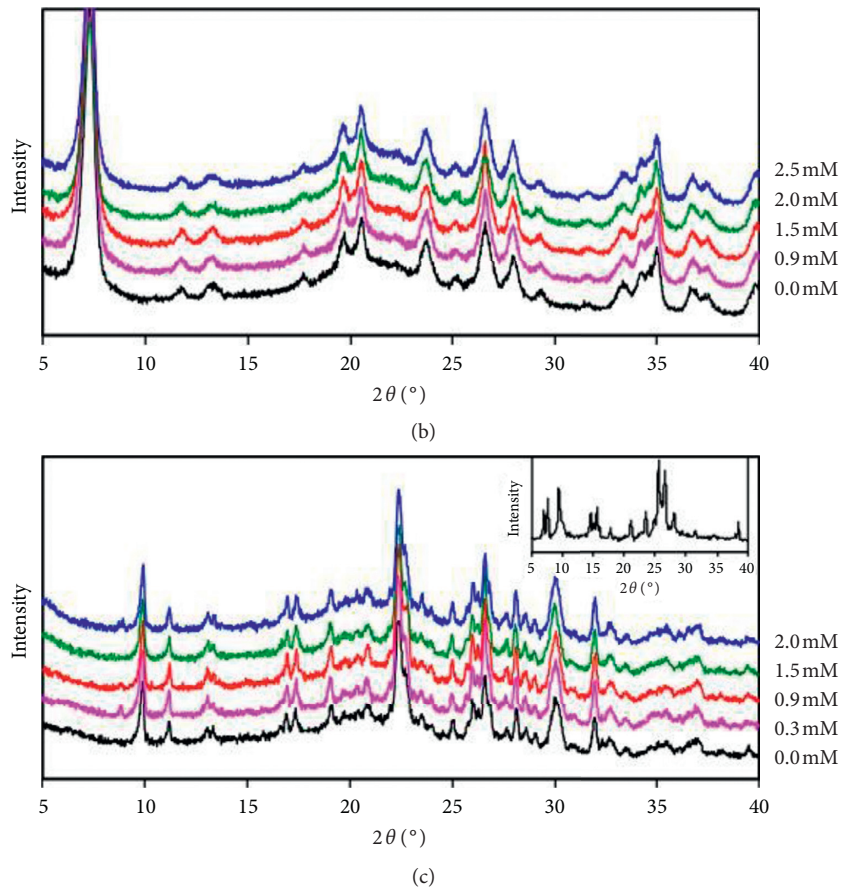

Figure 4: XRD patterns of PAL (a), SEP (b), and ZEO (c) after SO uptake from different initial SO concentrations. The inset in (c) is the XRD pattern of crystalline SO.

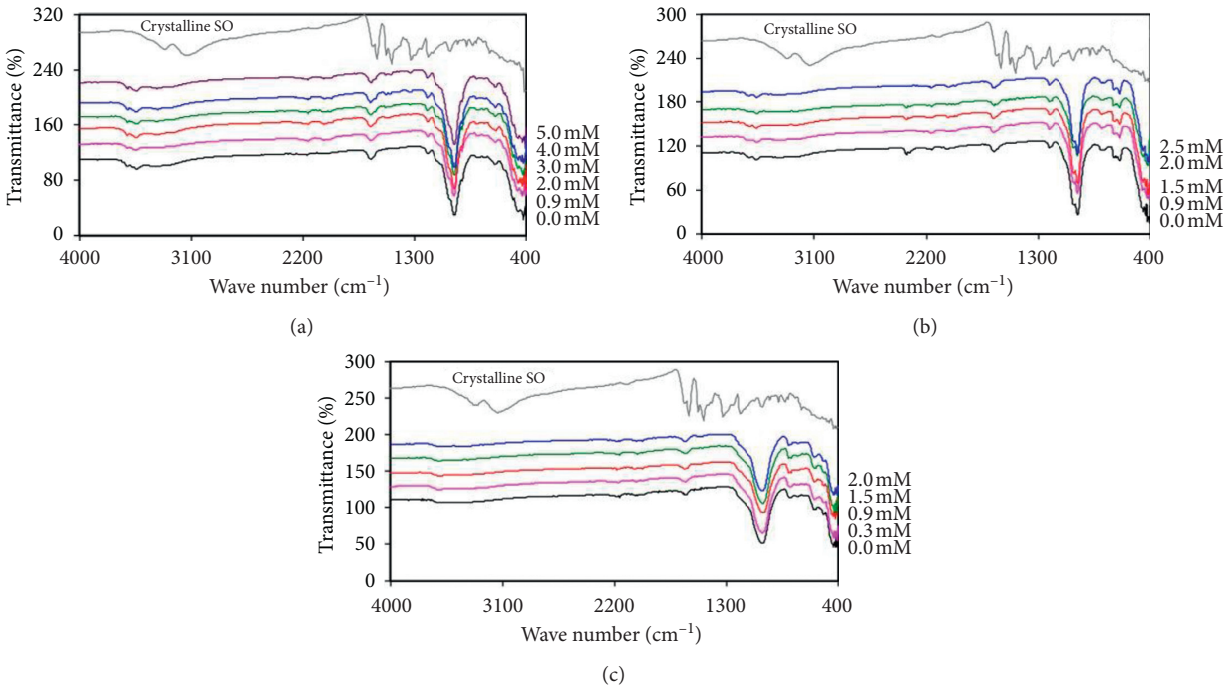

Figure 5: FTIR spectra of PAL (a), SEP (b), and ZEO (c) after SO sorption from different initial concentrations.

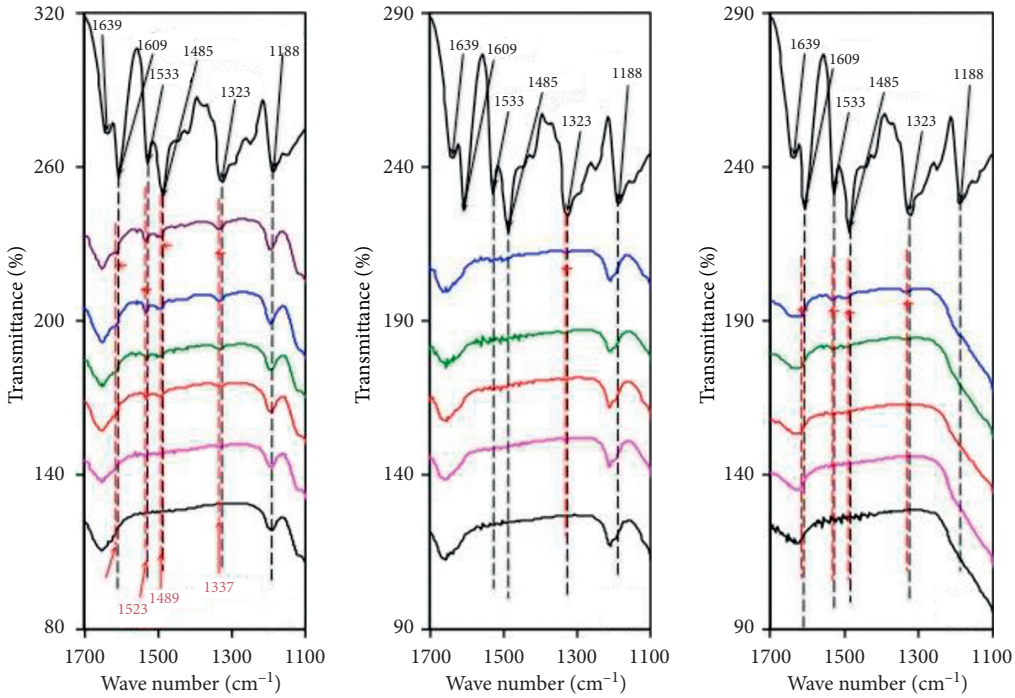

Figure 6: FTIR spectra of PAL (a), SEP (b), and ZEO (c) after SO sorption from different initial concentrations showing the enlargement at the wavenumbers of 1100–1700 cm^{-1}.

they shifted to 1339, 1491, 1533, and 1618 cm^{-1} (Figure 6(c)). These shifts, particularly the C = N stretching vibration band located at 1323 cm^{-1}, confirmed the participation of the C = N bond for the SO uptake on these mineral surfaces (Figure 6). Also, taking the consideration of the formula mass of 350 g/mol for SO, the sensitivity of FTIR for detection of sorbed SO is at the level of about 40 mmol/kg or 1.4%.

3.6. Molecular Dynamic Simulation. Molecular dynamic simulation was used to decipher the surface configuration of sorbed SO^+ cations at the sorption capacity for the minerals. For PAL and SEP, a supercell made of 2*bx*4*c* was used for the simulation, and the number of SO^+ cations used per supercell was calculated from the SO sorption capacity and the SSA of the minerals. The sorbed SO^+ cations formed a condensed monolayer configuration on PAL (Figure 7). In contrast, at the SO sorption maximum, the SO^+ cations formed monomers on SEP surfaces due to its much lower CEC and large SSA values (Figure 8). In both cases, the phenazine rings are parallel to the surfaces. ZEO is a granular mineral and supercells were made of 2*bx*4*c*, 2*ax*4*c*, and 2*ax*1.5*b*, and the number of SO molecules used per supercell was calculated from the SO sorption capacity and the SSA of the minerals. Multilayer or admicelle formation of SO on ZEO was obtained because of the very low SSA value of ZEO (Figures 9–11).

3.7. Discussion. The CEC values are 175 [25] and 15 [26] meq/kg for PAL and SEP, respectively, while the ECEC for ZEO is 90 meq/kg [28]. Meanwhile, the SO uptake capacity was 195, 45, and 79 mmol/kg for PAL, SEP, and ZEO, respectively (Figure 2(b)), strongly suggesting that cation exchange played a crucial role in SO removal. On the other hand, their SSA values are 173 [27] and 250 m^2/g [26] and the SSA is 15.7 m^2/g [28] for PAL, SEP, and ZEO, respectively. As the XRD results showed no changes in *d*-spacings for all minerals (Figure 4), it suggested that the uptake of SO was on the external surfaces of the minerals. Using the CEC and SSA values, the calculated area per SO^+ occupied at the uptake capacity is 1.5, 9.3, and 0.33 nm^2 for PAL, SEP, and ZEO, respectively. Meanwhile, the dimension of SO molecule is 1.16 nm long by 0.96 nm wide by 0.4 nm thick (Figure 1). The molecular simulation showed flat-lying SO^+ cations on {100} surface of PAL and SEP (Figures 7 and 8). Thus, a close monolayer packing of SO^+ on PAL and loose monomer packing of SO^+ on SEP suggested that the influence of SSA on SO uptake may not be critical. For ZEO, the SO sorption density was 0.33 nm^2 per SO^+ cation, much smaller than the dimension of SO. As SO may form dimers in solution and its dimer concentration increased with increasing SO concentration [34], formation of SO multilayer or admicelles on ZEO is extremely likely due to its limited SSA and large ECEC and was confirmed by the molecular dynamic simulation (Figures 9–11).

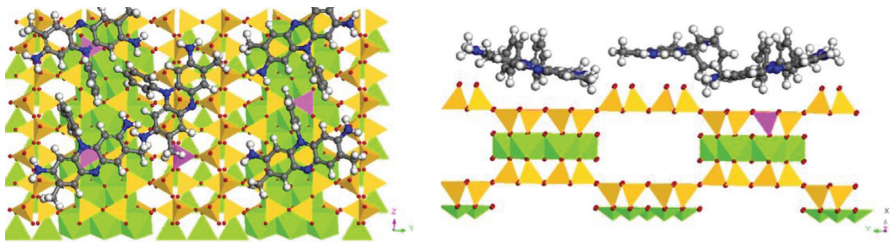

(a) (b)

Figure 7: Molecular dynamic simulation showing SO uptake on the {100} surface (a) and projection along [001] (b) of PAL with 4 Si replaced with 4 Al in the supercell.

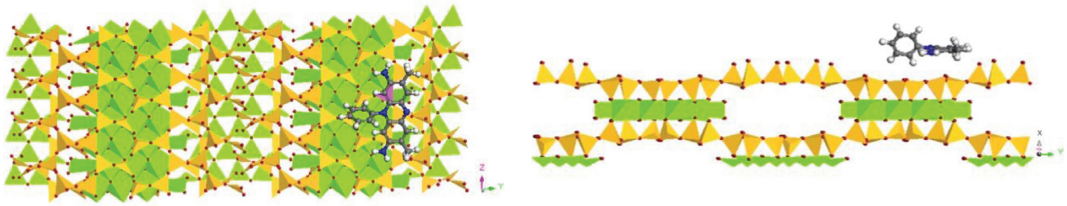

(a) (b)

Figure 8: Molecular dynamic simulation showing SO uptake on the {100} surface (a) and projection along [001] (b) of SEP with 1 Si replaced with 1 Al in the supercell.

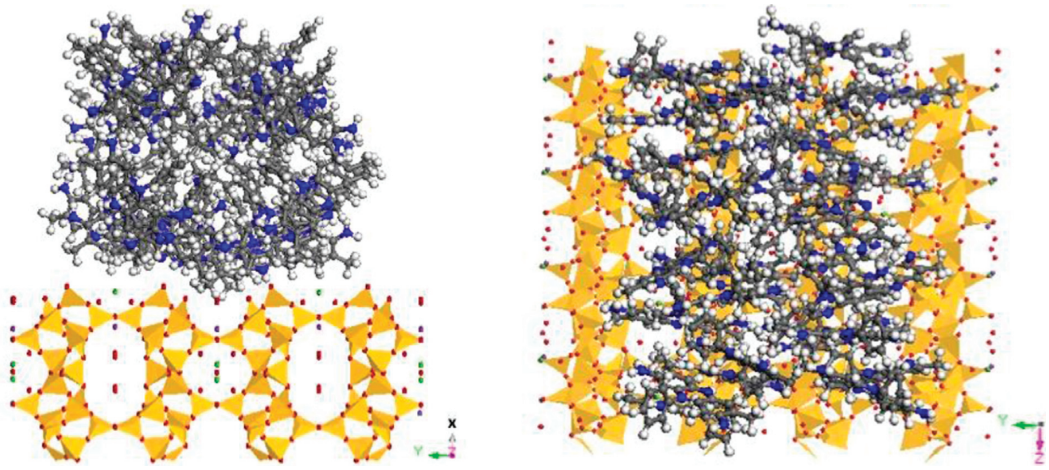

(a) (b)

Figure 9: Molecular dynamic simulation showing SO uptake on the {100} surface (a) and projection along [100] (b) of ZEO. Supercell is made of 2*bx*4*c*.

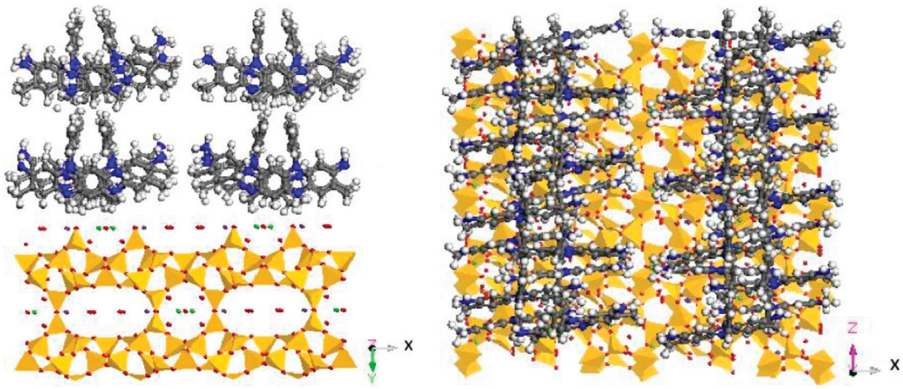

(a) (b)

Figure 10: Molecular dynamic simulation showing SO uptake on the {010} surface (a) and projection along [010] (b) of ZEO. Supercell is made of 2*a*x4*c*.

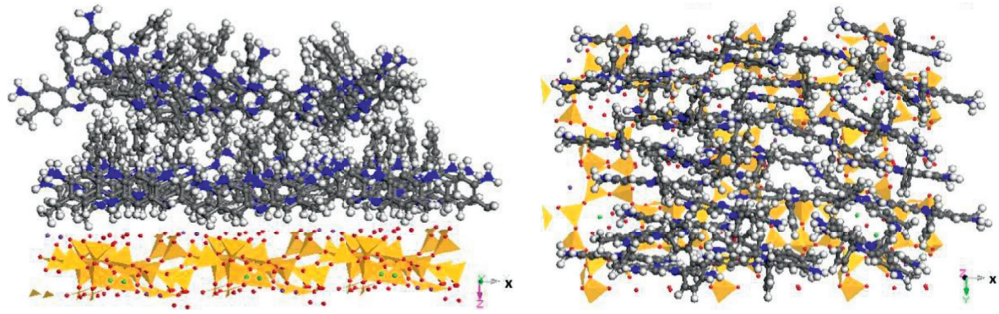

(a) (b)

Figure 11: Molecular dynamic simulation showing SO uptake on the {001} surface (a) and projection along [001] (b) of ZEO. Supercell is made of 2*a*x1.5*b*.

4. Conclusion

In this study, the sorptive removal of SO using fibrous clay minerals palygorskite and sepiolite and tectosilicate clinoptilolite zeolite was assessed under different physicochemical conditions. The results revealed that the SO removal capacity by these minerals was primarily controlled by their cation exchange capacity, suggesting cation exchange between SO^+ and inorganic cations played a key role in SO removal. Other physicochemical parameters such as equilibrium, solution pH, and ionic strength had minimal effect on SO removal. The sorbed SO^+ cations may form loosely packed monomers, densely packed monolayer, and multilayer or admicelle formations limited by the specific surface area of the minerals. The XRD results confirmed that the sorbed SO^+ cations were limited to the external surfaces of the minerals as the dimension of SO^+ is larger than the channel size of the minerals. The FTIR results suggested participation of N^+ in the benzene ring for the electrostatic interaction with negatively charged Si-O tetrahedral surface. The electrostatic interactions between SO^+ and negatively charged mineral surfaces and the SO^+ surface configurations on mineral surfaces were confirmed by molecular dynamic simulations. As a result, the clay minerals with high CEC and SSA values are good candidates for cationic dye removal from water.

Data Availability

The data used to support the findings of the current study are available from the corresponding author upon request.

Conflicts of Interest

The authors declare that they have no conflicts of interest.

Acknowledgments

This work was partially financially supported by the National Natural Science Foundation of China (41831288).

References

[1] S. Preethi, A. Sivasamy, S. Sivanesan, V. Ramamurthi, and G. Swaminathan, "Removal of safranin basic dye from aqueous solutions by adsorption onto corncob activated carbon," *Industrial & Engineering Chemistry Research*, vol. 45, no. 22, pp. 7627–7632, 2006.

[2] A. Tkaczyk, K. Mitrowska, and A. Posyniak, "Synthetic organic dyes as contaminants of the aquatic environment and their implications for ecosystems: a review," *Science of the Total Environment*, vol. 717, Article ID 137222, 2020.

[3] X.-L. Cao, Y.-N. Yan, F.-Y. Zhou, and S.-P. Sun, "Tailoring nanofiltration membranes for effective removing dye intermediates in complex dye-wastewater," *Journal of Membrane Science*, vol. 595, Article ID 117476, 2020.

[4] U. Shanker, M. Rani, and V. Jassal, "Degradation of hazardous organic dyes in water by nanomaterials," *Environmental Chemistry Letters*, vol. 15, no. 4, pp. 623–642, 2017.

[5] S. N. Singh, Ed., *Microbial Degradation of Synthetic Dyes in Wastewaters*, Springer, Berlin, Germany, 2014.

[6] A. H. Jawad, N. S. A. Mubarak, and A. S. Abdulhameed, "Hybrid crosslinked chitosan-epichlorohydrin/TiO_2 nanocomposite for reactive red 120 dye adsorption: kinetic, isotherm, thermodynamic, and mechanism study," *Journal of Polymers and the Environment*, vol. 28, no. 2, pp. 624–637, 2020.

[7] S. Kaur, S. Rani, R. K. Mahajan, M. Asif, and V. K. Gupta, "Synthesis and adsorption properties of mesoporous material for the removal of dye safranin: kinetics, equilibrium, and thermodynamics," *Journal of Industrial and Engineering Chemistry*, vol. 22, pp. 19–27, 2015.

[8] M. S. Thabet and A. M. Ismaiel, "Saudi Arabia natural clay: characterization, equilibrium, kinetics and thermodynamics models for elimination of textile dyes," *International Journal of Environmental Monitoring and Protection*, vol. 5, no. 2, pp. 31–39, 2018.

[9] V. Gómez, M. S. Larrechi, and M. P. Callao, "Kinetic and adsorption study of acid dye removal using activated carbon," *Chemosphere*, vol. 69, no. 7, pp. 1151–1158, 2007.

[10] N. Peinemann and A. K. Helmy, "Cation exchange capacities of safranin, toluidine and alizarin complexes with montmorillonite," *Soil Science*, vol. 164, no. 9, pp. 650–654, 1999.

[11] S. S. Al-Shahrani, "Removal of safranin dye from wastewater using Khulays natural bentonite," *Journal of King Abdulaziz University*, vol. 29, no. 1, pp. 49–58, 2018.

[12] K. O. Adebowale, B. I. Olu-Owolabi, and E. C. Chigbundu, "Removal of safranin-O from aqueous solution by adsorption onto kaolinite clay," *Journal of Encapsulation and Adsorption Sciences*, vol. 4, no. 3, pp. 89–104, 2014.

[13] R. G. Harris, J. D. Wells, and B. B. Johnson, "Selective adsorption of dyes and other organic molecules to kaolinite and oxide surfaces," *Colloids and Surfaces A: Physicochemical and Engineering Aspects*, vol. 180, no. 1-2, pp. 131–140, 2001.

[14] M. R. Abukhadra, M. A. El-Meligy, and A. M. El-Sherbeeny, "Evaluation and characterization of Egyptian ferruginous kaolinite as adsorbent and heterogeneous catalyst for effective removal of safranin-O cationic dye from water," *Arabian Journal of Geosciences*, vol. 13, no. 4, p. 169, 2020.

[15] E. Galán, "Properties and applications of palygorskite-sepiolite clays," *Clay Minerals*, vol. 31, no. 4, pp. 443–453, 1996.

[16] D. N. Taha, I. A. S. Samaka, and L. A. Mohammed, "Adsorptive removal of dye from industrial effluents using natural Iraqi palygorskite clay as low-cost adsorbent," *Journal of Asian Scientific Research*, vol. 3, no. 9, pp. 945–955, 2013.

[17] M. Fayazi, D. Afzali, M. A. Taher, A. Mostafavi, and V. K. Gupta, "Removal of safranin dye from aqueous solution using magnetic mesoporous clay: optimization study," *Journal of Molecular Liquids*, vol. 212, pp. 675–685, 2015.

[18] T. Rohani and M. S. Seyedghasemi, "Application of surfactant-coated magnetic zeolite NaA as a new sorbent to remove safranin O dye from aqueous solutions," *Bulgarian Chemical Communications*, vol. 49, pp. 323–328, 2017.

[19] V. Hovhannisyan, C. Y. Dong, and S. J. Chen, "Photodynamic dye adsorption and release performance of natural zeolite," *Scientific Reports*, vol. 7, Article ID 45503, 2017.

[20] M. Qiu, C. Qian, J. Xu, J. Wu, and G. Wang, "Studies on the adsorption of dyes into clinoptilolite," *Desalination*, vol. 243, no. 1–3, pp. 286–292, 2009.

[21] A. Badeenezhad, A. Azhdarpoor, S. Bahrami, and S. Yousefinejad, "Removal of methylene blue dye from aqueous solutions by natural clinoptilolite and clinoptilolite modified by iron oxide nanoparticles," *Molecular Simulation*, vol. 45, no. 7, pp. 564–571, 2019.

[22] M. R. Abukhadra and A. S. Mohamed, "Adsorption removal of safranin dye contaminants from water using various types of natural zeolite," *Silicon*, vol. 11, no. 3, pp. 1635–1647, 2019.

[23] R. Ebrahimi, A. Maleki, B. Shahmoradi et al., "Organic dye removal from aqueous media by using acid modified clinoptilolite," *Journal of Advances in Environmental Health Research*, vol. 6, no. 2, pp. 118–127, 2018.

[24] S. Bekkouche, S. Merouani, O. Hamdaoui, and M. Bouhelassa, "Efficient photocatalytic degradation of safranin O by integrating solar-UV/TiO_2/persulfate treatment: implication of sulfate radical in the oxidation process and effect of various water matrix components," *Journal of Photochemistry and Photobiology A: Chemistry*, vol. 345, pp. 80–91, 2017.

[25] D. Borden and R. F. Giese, "Baseline studies of the clay minerals society source clays: cation exchange capacity measurements by the ammonia-electrode method," *Clays and Clay Minerals*, vol. 49, no. 5, pp. 444-445, 2001.

[26] Z. Li, C. A. Willms, and K. Kniola, "Removal of anionic contaminants using surfactant-modified palygorskite and sepiolite," *Clays and Clay Minerals*, vol. 51, no. 4, pp. 445–451, 2003.

[27] A. U. Dogan, M. Dogan, M. Onal, Y. Sarikaya, A. Aburub, and D. E. Wurster, "Baseline studies of the clay minerals society source clays: specific surface area by the brunauer emmett teller (BET) method," *Clays and Clay Minerals*, vol. 54, no. 1, pp. 62–66, 2006.

[28] Z. Li and R. S. Bowman, "Counterion effects on the sorption of cationic surfactant and chromate on natural clinoptilolite," *Environmental Science & Technology*, vol. 31, no. 8, pp. 2407–2412, 1997.

[29] S. Manna, P. Das, and D. Roy, "Dye-containing wastewater treatment using treated jute," in *Waste Management and Resource Efficiency*, pp. 1263–1270, Springer, Singapore, Asia, 2019.

[30] F. Zhao and M. Sillanpää, "Cross-linked chitosan and β-cyclodextrin as functional adsorbents in water treatment," in *Advanced Water Treatment*, pp. 161–264, Elsevier, Amsterdam, Netherlands, 2020.

[31] R. Yang, D. Li, A. Li, and H. Yang, "Adsorption properties and mechanisms of palygorskite for removal of various ionic dyes from water," *Applied Clay Science*, vol. 151, pp. 20–28, 2018.

[32] P. Pereira, B. Ferreira, N. Oliveira et al., "Synthesis of zeolite a from metakaolin and its application in the adsorption of cationic dyes," *Applied Sciences*, vol. 8, no. 4, p. 608, 2018.

[33] S. Das and S. Barman, "Studies on removal of safranine-t and methyl orange dyes from aqueous solution using Nax zeolite synthesized from fly ash," *International Journal of Science, Environment and Technology*, vol. 2, no. 4, pp. 735–747, 2013.

[34] G. Balaji, R. K. Rekha, and A. Ramalingam, "Nonlinear characterization of safranin O dye for application in optical limiting," *Acta Physica Polonica A*, vol. 119, no. 3, pp. 359–363, 2011.

[35] N. Mansouri, N. Rikhtegar, H. A. Panahi, F. Atabi, and B. K. Shahraki, "Porosity, characterization and structural properties of natural zeolite-clinoptilolite-as a sorbent,"

Environment Protection Engineering, vol. 39, no. 1, pp. 139–152, 2013.

[36] M. K. Sahu and R. K. Patel, "Removal of safranin-O dye from aqueous solution using modified red mud: kinetics and equilibrium studies," *RSC Advances*, vol. 5, no. 96, pp. 78491–78501, 2015.

[37] S. A. Moon, B. K. Salunke, P. Saha, A. R. Deshmukh, and B. S. Kim, "Comparison of dye degradation potential of biosynthesized copper oxide, manganese dioxide, and silver nanoparticles using Kalopanax pictus plant extract," *Korean Journal of Chemical Engineering*, vol. 35, no. 3, pp. 702–708, 2018.

[38] H. Van Damme, M. Crespan, M. I. Cruz, and J. J. Fripiat, "Adsorption of safranine by Na^+, Ni^{2+} and Fe^{3+} montmorillonites," *Clays and Clay Minerals*, vol. 25, no. 1, pp. 19–25, 1977.